Available online at www.sciencedirect.com
ScienceDirect
Journal of Hazardous Materials 152 (2008) 241–249
Journal of Hazardous Materials
www.elsevier.com/locate/jhazmat

Prediction of ion-exchange column breakthrough curves by constant-pattern wave approach

I.-Hsien Lee, Yu-Chung Kuan, Jia-Ming Chern *

Department of Chemical Engineering, Tatung University, 40 Chungshan North Road, 3rd Sec., Taipei 10452, Taiwan

Received 11 July 2006; received in revised form 22 May 2007; accepted 26 June 2007
Available online 1 July 2007

Abstract

The release of heavy metals from industrial wastewaters represents one of major threats to environment. Compared with chemical precipitation method, fixed-bed ion-exchange process can effectively remove heavy metals from wastewaters and generate no hazardous sludge. In order to design and operate fixed-bed ion-exchange processes successfully, it is very important to understand the column dynamics. In this study, the column experiments for Cu^{2+}/H^+, Zn^{2+}/H^+, and Cd^{2+}/H^+ systems using Amberlite IR-120 were performed to measure the breakthrough curves under varying operating conditions. The experimental results showed that total cation concentration in the mobile-phase played a key role on the breakthrough curves; a higher feed concentration resulted in an earlier breakthrough. Furthermore, the column dynamics was also predicted by self-sharpening and constant-pattern wave models. The self-sharpening wave model assuming local ion-exchange equilibrium could provide a simple and quick estimation for the breakthrough volume, but the predicted breakthrough curves did not match the experimental data very well. On the contrary, the constant-pattern wave model using a constant driving force model for finite ion-exchange rate provided a better fit to the experimental data. The obtained liquid-phase mass transfer coefficient was correlated to the flow velocity and other operating parameters; the breakthrough curves under varying operating conditions could thus be predicted by the constant-pattern wave model using the correlation.

Keywords: Column dynamics; Constant-pattern wave; Heavy metal; Ion-exchange resin

1. Introduction

Untreated effluent wastewaters containing heavy metals from factories will damage the environment. Therefore, many methods such as chemical precipitation, activated carbon adsorption, ion-exchange, reverse osmosis, electrodialysis, and nanofiltration were used to remove heavy metals from wastewaters [1]. Because many methods are either not cost-effective or generate secondary pollution problems, adsorption or ion-exchange process using natural or synthetic materials to remove heavy metals from wastewater becomes relatively attractive [2–8]. Although direct addition of adsorbent to wastewater to remove heavy metals is quiet efficient, separation of the adsorbent from wastewater for repeated use is very time- and resource-consuming. Therefore, it seems to be more logical and cost-effective to remove heavy metals from industrial wastewaters by using fixed-bed operations instead of batch operations [9–13].

Fixed-bed ion-exchange system packed with suitable resin particles in a column can treat heavy metal effluent by entering the wastewater from the top and leaving at the bottom of the column. During downward flow, the heavy metals in the mobile-phase are exchanged onto the stationary resin particles in the bed that are pre-saturated with the less favorable ion such as H^+. From the top to the bottom, the resins in each layer are converted from hydrogen form to metal form and lose their exchangeable ability. If the wastewater continuously feeds into the column, the exchanged zone migrates downwards until the effluent metal concentration becomes the same as the influent concentration. When column breakthrough takes place, the heavy metal-saturated column must be backwashed, regenerated, and rinsed before next utilization cycle [14]. From the standpoint of heavy metal removal only, the above operating mode is simple and has been widely used in water and wastewater treatment practice. However, if heavy metal separation and recovery are desired, we need to know what kind of heavy metal will exit an ion-exchange column at what time period. Then we can collect the effluent solutions and separate different heavy metals. In order to know what kind of metal ion

* Corresponding author. Tel.: +886 2 27002737x23; fax: +886 2 27079528.
E-mail address: jmchern@ttu.edu.tw (J.-M. Chern).

0304-3894/$ – see front matter © 2007 Elsevier B.V. All rights reserved.
doi:10.1016/j.jhazmat.2007.06.098

Nomenclature

A	cross-section area of column (cm^2)
C	total cation concentration in the mobile-phase (meq./L)
$\bar{C}$	total cation concentration or capacity in the stationary-phase (meq./g resin)
C_H	hydrogen ion concentration in the mobile-phase (meq./L)
$\bar{C}_H$	hydrogen ion concentration in the stationary-phase (meq./g resin)
C_M	metal ion concentration in the mobile-phase (meq./L)
$\bar{C}_M$	metal ion concentration in the stationary-phase (meq./g resin)
C_{MF}	feed metal ion concentration in the mobile-phase (meq./L)
k_1	model coefficient defined in Eq. (17) (h^{-1})
k_2	model coefficient defined in Eq. (17) ($cm^{-3/2}\,h^{-1/2}$)
k_2'	model coefficient defined in Eq. (18) ($cm^{-1/2}\,h^{-1/2}$)
K_La	volumetric mass-transfer coefficient in liquid phase defined in Eq. (8) (h^{-1})
K_{MH}	equilibrium constant defined in Eq. (7) (g resin/L solution)
K'_{MH}	modified equilibrium constant defined in Eq. (6) (–)
L	length of ion-exchange resin bed (cm)
m	slope of the linearization defined in Eq. (15) (cm^3)
pH_0	initial feed pH in the mobile-phase (–)
t	time (h)
$t_{1/2}$	half time at $x_M = 1/2$ (h)
u_0	linear velocity of the mobile-phase fluid (cm/h)
u_{x_M}	concentration fraction wave velocity of a self-sharpening wave (cm/h)
V	cumulative effluent volume (mL)
$V_{1/2}$	cumulative effluent volume at $x_M = 1/2$ (mL)
V_B	ion-exchange bed volume (mL)
V_{BK}	breakthrough volume by self-sharpening wave (mL)
x_H	hydrogen ion equivalence fraction in the mobile-phase (–)
x_M	metal equivalence fraction in the mobile-phase (–)
x_{MF}	feed metal equivalence fraction in the mobile-phase (–)
x_{MP}	presaturation metal equivalence fraction in the mobile-phase (–)
x_M^*	equilibrium metal equivalence fraction in the mobile-phase (–)
y_H	hydrogen ion equivalence fraction in the stationary-phase (–)
y_M	metal equivalence fraction in the stationary-phase (–)
y_{MF}	feed metal equivalence fraction in the stationary-phase (–)
y_{MP}	presaturation metal equivalence fraction in the stationary-phase (–)
Z	distance from the inlet of mobile-phase (cm)

Greek letters

ε	void fraction of ion-exchange resin bed (–)
ρ	density of ion-exchange resin (g resin/cm^3)
τ	adjusted time, $\tau = t - Z/u_x$ (h)

exits an ion-exchange column at what time period, we need to know the dynamic behavior of the column.

Although a variety of models were available to predict the fixed-bed dynamics [15–21], the non-linear wave propagation theory provided a simple method to estimate the column breakthrough times for any types of adsorption isotherms [22–24]. Because the needed assumptions, infinite mass-transfer rate and local equilibrium, of the non-linear wave propagation theory are not always met for fixed-bed operations, a constant-pattern wave approach was proposed to predict the breakthrough curves of fixed-bed adsorption processes with Langmuir or Freundlich adsorption isotherms [25]. The constant-pattern wave approach was adopted to model the breakthrough curves of fixed-bed processes to remove organic pollutants such as phenols, *p*-nitrophenol and acid dye [26–29]. The Langmuir and Freundlich adsorption isotherm models, although commonly used in adsorption processes, are not suitable for ion-exchange processes especially when the exchanged ions possess different valences, e.g. heavy metal and hydrogen ion. According to our previous results [30], reversible reaction model using a equilibrium constant to express the ion-exchange equilibriums of M^{2+}/H^+ system can not only describe the ion-exchange equilibriums satisfactorily but also provide a closer fit to the ion-exchange kinetic data. This study therefore focuses on extending the constant-pattern wave approach to predict the breakthrough curves of heavy metal ion-exchange processes using the reversible reaction model for the ion-exchange equilibriums of Cu^{2+}/H^+, Zn^{2+}/H^+, and Cd^{2+}/H^+ systems.

2. Theory

The column dynamic behavior of an ion-exchange process can be described by a set of differential equations coupled with a set of algebraic equations. Consider an ion-exchange system with two exchangeable cations, H^+ and M^{2+}, the governing equation of the column dynamics for heavy metal M^{2+} is:

$$\left(\frac{1-\varepsilon}{\varepsilon}\right)\left(\frac{\bar{C}}{C}\right)\frac{\rho\partial y_M}{\partial t} + \frac{\partial x_M}{\partial t} + u_0\frac{\partial x_M}{\partial Z} = 0 \quad (1)$$

where x_M is the heavy metal equivalence fraction in the mobile-phase, y_M is the heavy metal equivalence fraction in the stationary-phase, C is the total cation (heavy metal plus hydrogen) concentration in the mobile-phase, $\bar{C}$ is the total

cation concentration in the stationary-phase or the ion-exchanger capacity, ε is the void fraction of the ion-exchange bed, u_0 is the linear velocity of the mobile-phase fluid, t is the operation time, ρ is the density of ion-exchange resin and Z is the distance from the inlet of the mobile phase. Eq. (1) is basically the unsteady-state mass balance of the heavy metal M^{2+}. The assumptions associated with Eq. (1) are:

- No chemical reactions occur in the column.
- Exclusion of co-ions and non-ionic species from the resin interior.
- No shrinking or swelling of resin.
- The flow pattern is ideal plug flow.
- Only mass transfer by convection is significant.
- The temperature in the column is uniform and invariant with time.
- The flow rate is constant and invariant with the column position.
- Unity activity coefficients.

Similar to the adsorption process, assuming local equilibrium and using the definition of the concentration wave velocity and the chain rule of calculus, the self-sharpening wave velocity [25,31–33] can be expressed as follows:

$$u_{x_M} = \frac{u_0}{1 + \rho[(1-\varepsilon)/\varepsilon](\bar{C}/C)(\Delta y_M/\Delta x_M)_Z} \tag{2}$$

If the concentration fraction wave velocity is known, the dynamics of ion-exchange column can be easily predicted. Finally, the breakthrough curve of a self-sharpening ion-exchange wave can be calculated by the following equation [25]:

$$\begin{cases} x_M = x_{MP} & \text{for} \quad 0 \le V \le V_{BK} \\ x_M = x_{MF} & \text{for} \quad V \ge V_{BK} \end{cases} \tag{3}$$

where the subscripts F and P represent the feed and presaturation conditions, respectively; V_{BK} is the breakthrough volume calculated by the self-sharpening wave model:

$$V_{BK} = V_B \left[\varepsilon + \rho(1-\varepsilon) \left(\frac{\bar{C}}{C}\right) \left(\frac{y_{MF} - y_{MP}}{x_{MF} - x_{MP}}\right) \right] \tag{4}$$

where V_B is the resin bed volume.

In Eq. (4), the heavy metal equivalence fraction in the resin phase y_{MF} can be expressed as a function of the metal fraction in the solution phase [30]:

$$y_M = 1 - \frac{-1 + \sqrt{1 + 4K'_{MH} x_M/(1-x_M)^2}}{2K'_{MH} x_M/(1-x_M)^2} \tag{5}$$

where K'_{MH} is the modified equilibrium constant defined as:

$$K'_{MH} = K_{MH}\frac{\bar{C}}{C} = \left(\frac{y_M}{x_M}\right)\left(\frac{x_H}{y_H}\right)^2 \tag{6}$$

In Eq. (6), K_{MH} is the true equilibrium constant defined by mass action law for the ion-exchange process of $M^{2+} + 2\overline{H^+} \leftrightarrow \overline{M^{2+}} + 2H^+$:

$$K_{MH} = \left(\frac{\overline{C}_M}{C_M}\right) \cdot \left(\frac{C_H}{\overline{C_H}}\right)^2 \tag{7}$$

As shown by the previous study [25], the prediction of the breakthrough curve by Eq. (4) is based on the local equilibrium assumption. Under practical operating conditions, the local equilibrium assumption may not be justified due to limited mass-transfer rate. In this case, the self-sharpening wave will eventually evolve into a constant-pattern wave moving at a constant velocity.

The ion-exchange rate in Eq. (1) can be described by a constant driving force model using an overall liquid-phase mass-transfer coefficient [34]:

$$\left(\frac{1-\varepsilon}{\varepsilon}\right)\left(\frac{\bar{C}}{C}\right)\frac{\rho \partial y_M}{\partial t} = K_L a(x_M - x^*_M) \tag{8}$$

where $K_L a$ is the overall mass-transfer coefficient; x^*_M is the mobile-phase heavy metal equivalence fraction in equilibrium with the stationary-phase heavy metal equivalence fraction y_M.

During the propagation of the constant-pattern wave, the ratio of the heavy metal concentration in the stationary- and mobile-phases is constant:

$$\frac{y_M}{x_M} = \frac{y_{MF}}{x_{MF}} = \text{constant} \tag{9}$$

Substituting y_M with $y_{MF}x_M/x_{MF}$ into Eq. (8), the mobile-phase concentration can be expressed as a unique function of the adjusted time defined as $\tau = t - Z/u_{x_M}$. The breakthrough curve can thus be predicted by the following equation [25]:

$$t = t_{1/2} + \left(\frac{1-\varepsilon}{\varepsilon}\right)\left(\frac{\bar{C}}{C}\right)\frac{y_{MF}\rho}{x_{MF}K_L a} \times \int_{1/2}^{x_M} \frac{1}{x_M - g(y_{MF}x_M/x_{MF})}\,dx_M \tag{10}$$

where g is the reverse function of Eq. (5), i.e., $x^*_M = g(y_M)$.

$$x^*_M = 1 + \frac{K'_{MH}}{2y_M}(1-y_M)^2 - \frac{1-y_M}{2}\sqrt{\frac{4K'_{MH}}{y_M} + \frac{K'^2_{MH}}{y^2_M}(1-y_M)^2} \tag{11}$$

In fixed-bed operations the cumulative effluent volume, V equaling $u_0\varepsilon At$ is usually used instead of the operating time:

$$V = V_{1/2} + (1-\varepsilon)\left(\frac{\bar{C}}{C}\right)\left(\frac{y_{MF}}{x_{MF}}\right)\frac{u_0 A\rho}{K_L a} \times \int_{1/2}^{x_M} \frac{1}{x_M - g(y_{MF}x_M/x_{MF})}\,dx_M \tag{12}$$

where $V_{1/2}$ is the cumulative effluent volume when the effluent x_M equals 1/2.

Combining Eqs. (11) and (12) leads to the following equation that can be used to predict the breakthrough curves of fixed-bed

ion-exchange processes:

$$V = V_{1/2} + (1-\varepsilon)(\bar{C}/C)\left(\frac{y_{MF}}{x_{MF}}\right)\frac{u_0 A\rho}{K_L a}\int_{1/2}^{x_M} f(x_M)\,dx_M \quad (13)$$

where $f(x_M)$ is a function of the metal equivalence fraction in the solution phase, x_M:

$$f(x_M) = \frac{1}{x_M - 1 - (K'_{MH}x_{MF}/2x_M y_{MF})(1-(y_{MF}/x_{MF})x_M)^2[1-\sqrt{1+4x_M y_{MF}/K'_{MH}x_{MF}(1-(y_{MF}/x_{MF})x_M)^{-2}}]} \quad (14)$$

3. Materials and methods

3.1. Experimental materials

The strong acid cationic exchange resin, Amberlite IR-120 (Rohm Haas Corp., USA) was used in this study. The resin used has a true density of 1.26 g/cm^3, particle size ranges from 0.30 to 0.59 mm, operating pH ranges from 0 to 14, and moisture content ranges from 48 to 55 %. Before the column experiments, the ion-exchange resin was first screened by passing through a series of sieves to narrow the particle size distribution. The screened ion-exchange resins were acid-conditioned with 1N HCl (Yakuri Pure Chemicals Corp., Japan) several times to convert the exchange sites to the desired H^+ form. The heavy metal solutions were prepared by dissolving copper nitrate, zinc nitrate, and cadmium nitrate (Wako Pure Chemicals Corp., Japan) in ultra pure deionized water provided by Synergy Water System (Millipore Corp., USA).

3.2. Experimental procedures

About 3 g of the conditioned resin was placed in a glass column and a known amount of standard 0.1N sodium hydroxide solution was fed to the column at a low flow rate to determine the ion-exchange capacity of the resin. The capacity of the ion-exchange resin was determined to be 6.38 ± 0.49 meq./g.

The column dynamic experiments were carried out in a jacketed-type fixed-bed column with inner diameter of 1.0 cm and the temperature was controlled at 298 K. At the bottom of the column, a glass-wool membrane was equipped to prevent the loss of resin. Desired amounts of resin were carefully added to the column; the entrapped air was removed by fluidizing the column with deionized water. After finishing bed fluidization, the re-settle down resin particles were rinsed with downflow deionized water. To start a column experiment, the heavy metal solution with desired metal concentration was fed to the top of the column. A metering pump (Tokyo Rikakikai Corp., MP-3N) was used to control the flow rate at about 5–7 BV/h and a fraction collector (ISCO, Retriever 500) was used to collect the samples for metal concentration analysis by an atomic absorption spectrophotometer (Varian, Model 3000). The effluent solution samples were instantly measured by a pH meter (Radiometer Co., PHM240) in order to observe the column breakthrough. Since the effect of bed length on the adsorption breakthrough curve has been studied and known [25], only the effects of total cation concentration and flow rate are focused in this study. All the column experimental conditions are summarized in Table 1.

4. Results and discussion

4.1. Self-sharpening wave vs. constant-pattern wave approach

Fig. 1a shows a typical breakthrough curve of copper with open circles representing the experimental data, dashed curve representing the breakthrough curve predicted by the self-sharpening wave model, and solid curve representing the breakthrough curve predicted by the constant-pattern wave model. The true equilibrium constants, K_{CuH} = 40.43 g/L, K_{ZnH} = 37.48 g/L and K_{CdH} = 37.44 g/L used in model calculations were determined in our previous study [30]. As is shown by Eq. (3), the breakthrough curve is a "step"; the effluent heavy metal concentration equals the column pre-saturation concentration (zero in this study) for cumulative effluent volume less than the breakthrough volume and climbs to the feed concentration at and beyond the breakthrough volume. Although the

Table 1
Experimental conditions of column tests

Run	System (M^{2+}/H^+)	Mobile phase concentration (meq./L)	Feed metal fraction	Feed pH	Bed void fraction	Bed length (cm)	Linear velocity (cm/h)
1	M = Cu	1.0	0.999	5.90	0.4	5.0	63.8
2	M = Cu	18.3	0.982	3.49	0.4	5.0	56.3
3	M = Cu	43.7	0.999	4.74	0.4	5.0	77.5
4	M = Zn	1.0	0.998	5.84	0.4	5.0	63.8
5	M = Zn	16.5	0.999	4.87	0.4	5.0	68.2
6	M = Zn	30.2	0.999	4.78	0.4	5.0	81.3
7	M = Cd	1.0	0.998	5.71	0.4	5.0	63.8
8	M = Cd	19.1	0.996	4.15	0.4	5.0	65.0
9	M = Cd	27.1	0.999	4.81	0.4	5.0	70.0
10	M = Cu	29.3	0.625	1.96	0.4	5.0	51.2
11	M = Zn	27.7	0.699	2.08	0.4	5.0	86.6
12	M = Cd	28.1	0.676	2.04	0.4	5.0	61.1

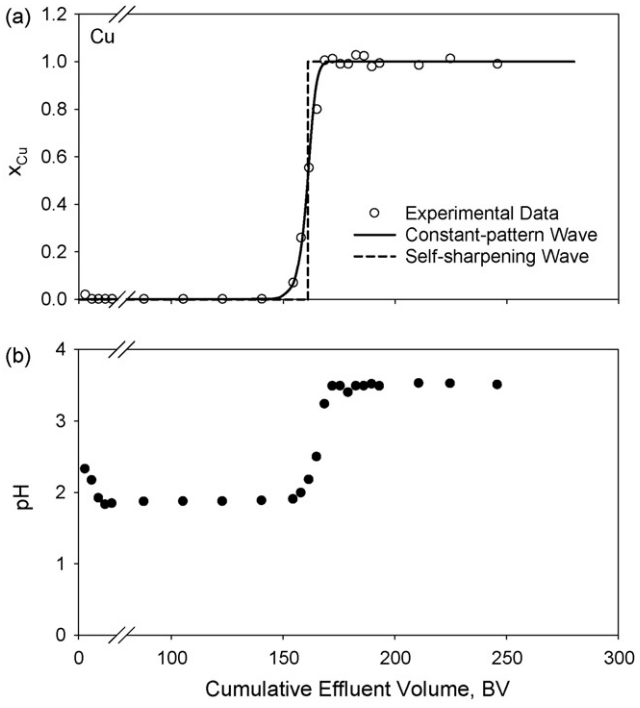

Fig. 1. Ion-exchange column breakthrough curves demonstrated by (a) experimental data and curves predicted by constant-pattern wave and self-sharpening wave models and (b) effluent pH and hydrogen concentration.

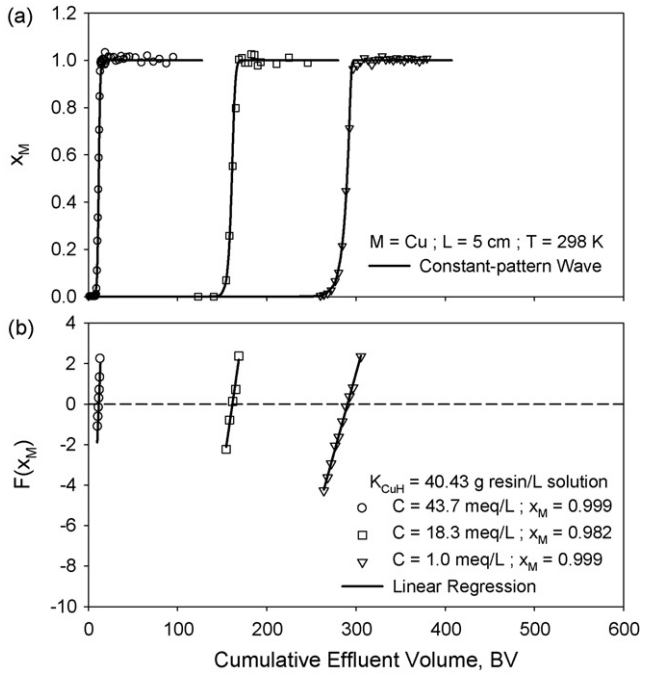

Fig. 2. Ion-exchange column breakthrough curves of Cu^{2+}/H^+ system demonstrated by (a) experimental data and curves predicted by constant-pattern wave model and (b) linearization of $F(x_M)$ vs. cumulative effluent volume.

self-sharpening wave model can roughly and rapidly estimate the breakthrough volume, the solid curve in Fig. 1a predicted by the constant-pattern wave model obviously fits the experimental data much better. The discrepancy of model prediction capability mainly depends on the model assumptions. Assuming local ion-exchange equilibrium in the self-sharpening wave model implies that the mass-transfer rate is infinitive. To avoid this unreasonable assumption, the constant-pattern wave model adopts a finite mass-transfer rate and therefore provides a better fit to the breakthrough curve.

Fig. 1b shows the effluent pH history. Comparing Fig. 1a and b, we can find the effluent pH has the same trend as the copper concentration breakthrough curve. Because hydrogen ion is exchanged with the copper ion and released into the solution phase, the hydrogen ion concentration will remain at a higher level before breakthrough. Then, it suddenly drops to the feed concentration at and beyond the breakthrough volume, according to the self-sharpening wave theory. Probably due to complex reaction of copper ion and hydroxide ion in the solution, the experimental hydrogen concentration and pH curves do not perfectly fit the model-predicted curves. Nevertheless, the sharp increase of the effluent pH can serve as a good indicator for breakthrough in fixed-bed ion-exchange operation.

4.2. Prediction of breakthrough curve by constant-pattern wave model

For a given effluent heavy metal equivalence fraction x_M, we can substitute Eq. (14) into Eq. (13) and use a numerical integration method to calculate the accumulative effluent volume if the overall liquid-phase mass-transfer coefficient K_La is known. The overall liquid-phase mass-transfer coefficient depends on the hydrodynamics in the fixed bed and can be determined by the following procedure [25]:

- Use Simpson's integration method to obtain the integration term in Eq. (13)
- Re-defined a new function $F(x_M)$ with a reciprocal slope m:

$$F(x_M) = \frac{1}{m}(V - V_{1/2}) \tag{15}$$

where

$$m = (1-\varepsilon)\left(\frac{\bar{C}}{C}\right)\left(\frac{y_{MF}}{x_{MF}}\right)\frac{u_0 A\rho}{K_L a} \tag{16}$$

- Plot $F(x_M)$ versus V and use linear regression to obtain m and $V_{1/2}$.

The slope and intercept of the linear plots shown in Fig. 2b were used to calculate the overall mass-transfer coefficient K_La and the half breakthrough volume $V_{1/2}$ of the Cu^{2+}/H^+ ion-exchange column tests, respectively. In practice, only the data points near the half breakthrough volume $V_{1/2}$ were used for the calculations. The very good linearity for run 1 to run 3 shown in Fig. 2b suggests the methodology is also applicable to the ion-exchange column tests. Using the obtained model parameters, $V_{1/2}$ and K_La, the breakthrough curves were calculated by Eq. (13) and the results are shown in Fig. 2a. As shown by Fig. 2a, the constant-pattern wave model predicts the breakthrough curves of Cu^{2+}/H^+ ion-exchange column tests satisfactorily. Similarly, the results for Zn^{2+}/H^+ and Cd^{2+}/H^+ ion-exchange systems are shown in Figs. 3 and 4, respectively.

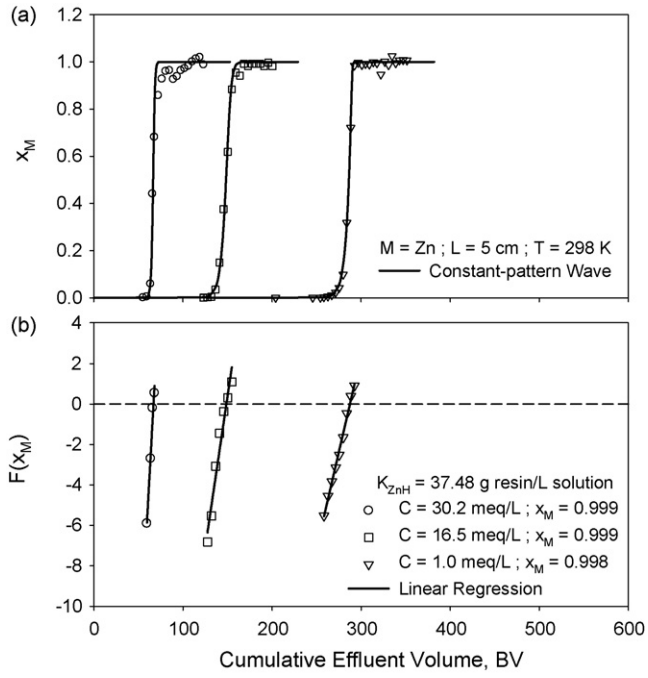

Fig. 3. Ion-exchange column breakthrough curves of Zn^{2+}/H^+ system demonstrated by (a) experimental data and curves predicted by constant-pattern wave model and (b) linearization of $F(x_M)$ vs. cumulative effluent volume.

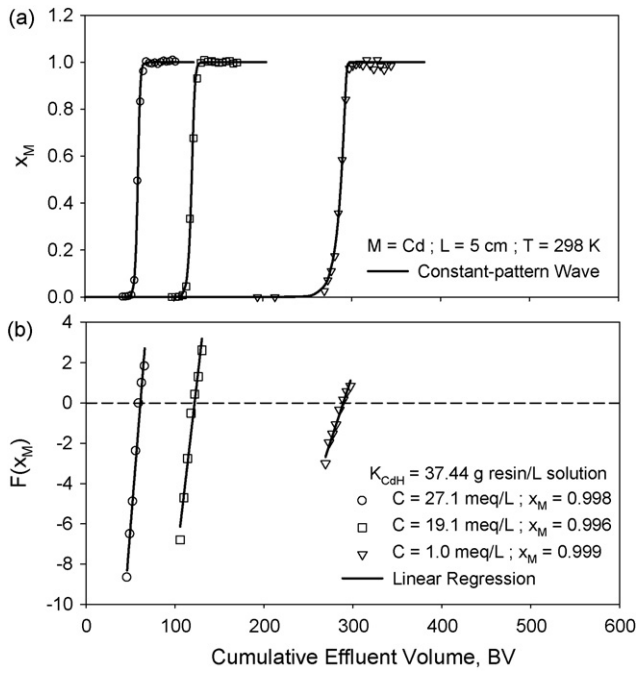

Fig. 4. Ion-exchange column breakthrough curves of Cd^{2+}/H^+ system demonstrated by (a) experimental data and curves predicted by constant-pattern wave model and (b) linearization of $F(x_M)$ vs. cumulative effluent volume.

4.3. Comparison of $V_{1/2}$ and breakthrough volume

The model parameters, $V_{1/2}$ and K_La for all the test runs are summarized in Table 2. Also shown in Table 2 are the breakthrough volumes calculated by the self-sharpening wave model, Eq. (4). For comparison, the breakthrough volume predicted by the self-sharpening wave model and the half breakthrough volume at $x_M = 1/2$ obtained by the constant-pattern wave model are listed in Table 2. As is shown by Table 2, the half breakthrough volume $V_{1/2}$ and the breakthrough volume V_{BK} are basically the same. Therefore, the half breakthrough volume $V_{1/2}$ of the constant-pattern wave model can be easily estimated by Eq. (4), the self-sharpening wave model.

4.4. Correlation of volumetric mass-transfer coefficient

In order to estimate the overall mass-transfer coefficients in ion-exchange column operations, a correlation for the overall mass-transfer coefficient as a function of operating parameters is highly desired. Chern and Chien used a correlation to esti-

Table 2
Model parameters for copper, zinc and cadmium[a]

Experimental condition				Constant-pattern wave			SS[b] wave
M^{2+}/H^+	C (meq./L)	x_{MF} (–)	u_0 (cm/h)	K_La (h^{-1})		$V_{1/2}$ (BV)	V_{BK} (BV)
				Experimental	Calculated[c]		
M = Cu	1.0	0.999	63.8	1.56	1.77	290.2	288.7
	18.3	0.982	56.3	1.12	1.66	161.2	161.9
	43.7	0.999	77.5	1.78	1.95	11.7	13.4
	29.3	0.625	51.2	0.97	1.58	176.1	171.6
M = Zn	1.0	0.998	63.8	1.80	1.54	286.3	284.6
	16.5	0.999	68.2	1.04	1.59	148.2	145.2
	30.2	0.999	81.3	1.20	1.73	66.2	69.9
	27.7	0.699	86.6	1.26	1.78	87.3	89.3
M = Cd	1.0	0.998	63.8	1.27	1.42	288.1	285.6
	19.1	0.996	65.0	1.15	1.43	120.1	120.2
	27.1	0.999	70.0	1.34	1.49	59.5	59.4
	28.1	0.676	61.1	0.84	1.39	122.5	120.2

[a] Resin properties $\varepsilon = 0.4$, $\rho = 1.26$ g/cm^3, $\bar{C} = 6.38$ meq./g $K_{CuH} = 40.43$ g/L, $K_{ZnH} = 37.48$ g/L, $K_{CdH} = 37.44$ g/L.
[b] Self-sharpening wave model.
[c] K_La is calculated from Eq. (16).

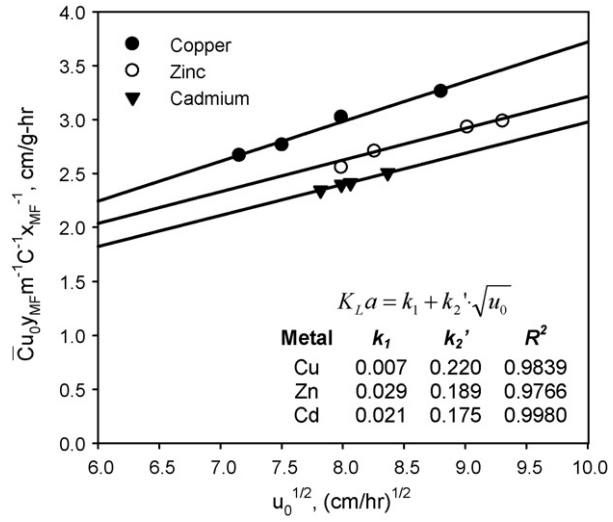

Fig. 5. Linear plots of the modified volumetric mass-transfer coefficient.

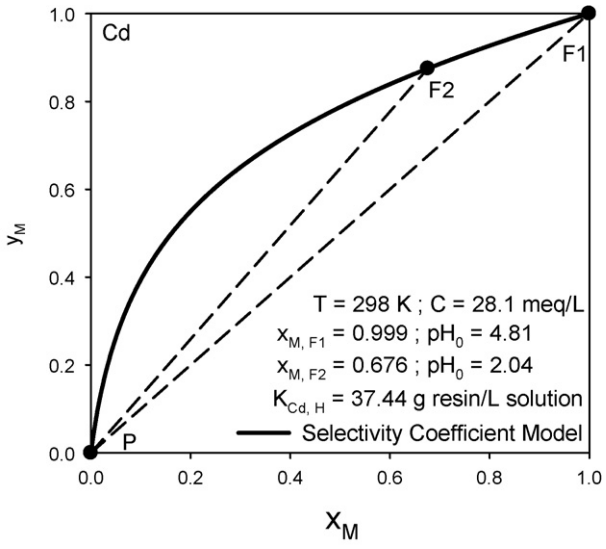

Fig. 6. Different column operating conditions on ion-exchange equilibrium plot.

mate the individual liquid-film coefficient of phenol in activated carbon bed and found that solid-phase mass transfer resistance could not be neglected; therefore they proposed an empirical correlation of the overall liquid-phase mass-transfer coefficient for activated carbon adsorption process [25]:

$$K_L a = k_1 + k_2 Q^{1/2} \tag{17}$$

where Q is the feed flow rate that can be expressed as the linear velocity of the mobile-phase times the bed cross-sectional area. The overall liquid-phase mass-transfer coefficient can then be expressed as a function of the linear velocity of the mobile-phase:

$$K_L a = k_1 + k_2' \sqrt{u_0} \tag{18}$$

Substituting Eq. (18) to Eq. (16) leads to

$$\frac{\bar{C}u_0 y_{MF}}{mCx_{MF}} = \frac{1}{A\rho(1-\varepsilon)}(k_1 + k_2'\sqrt{u_0}) \tag{19}$$

According to Eq. (18), the plot of $\bar{C}u_0 y_{MF}/mCx_{MF}$ versus $\sqrt{u_0}$ should be linear if the correlation, Eq. (18) is adequate. Fig. 5 shows that the plots of $\bar{C}u_0 y_{MF}/mCx_{MF}$ versus $\sqrt{u_0}$ for Cu^{2+}/H^+, Zn^{2+}/H^+, and Cd^{2+}/H^+ ion-exchange systems are indeed linear and the R^2 values are close to unity. Using the correlation, Eq. (19), for given fluid velocity, feed composition, total cation concentration in the mobile-phase, and resin bed properties we can calculate the reciprocal slope m with which the overall mass-transfer coefficient $K_L a$ can be calculated by Eq. (16). Once the half breakthrough volume $V_{1/2}$ is estimated by Eq. (4) for the breakthrough volume V_{BK}, the breakthrough curve can be predicted by Eq. (13) using the calculated overall mass-transfer coefficient $K_L a$.

4.5. Effect of feed metal concentration and pH

It is quite common that the effluent metal concentration and pH in wastewater may vary with manufacturing process. The ion-exchange column dynamics is thus different for different feed metal concentrations and pHs according to the wave propagation models. To understand the effects of the feed metal concentration and pH on the breakthrough curve, it is important to note that the equilibrium constant based on the mass action

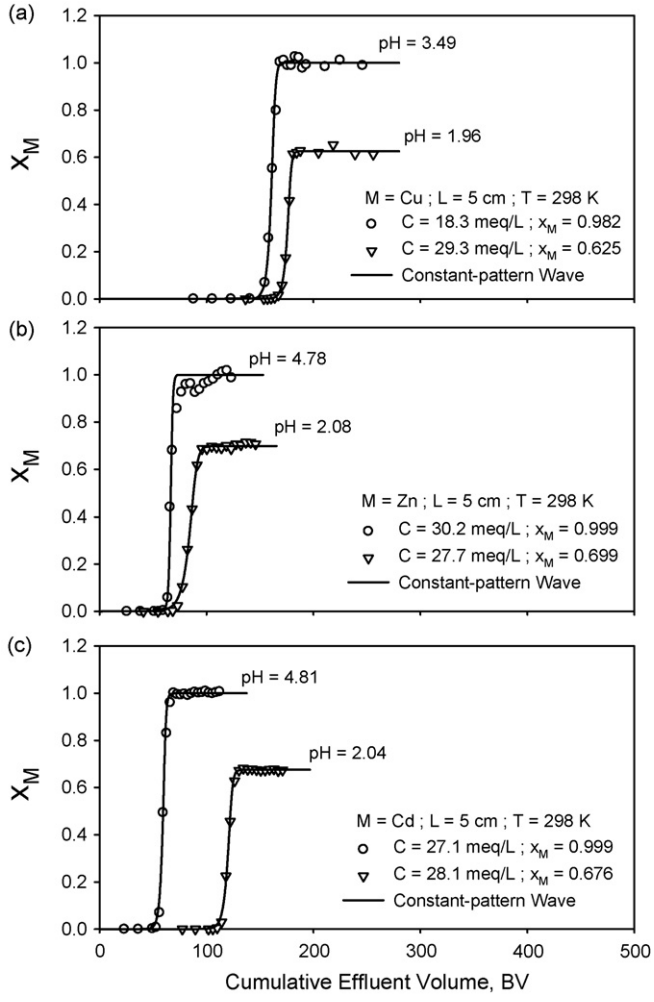

Fig. 7. Effect of feed pH on the ion-exchange breakthrough curves.

law, K_{MH} is a true constant while the modified equilibrium constant K'_{MH} defined in Eq. (6) depends on the total mobile-phase concentration. According to Eq. (4), the breakthrough volume V_{BK} ($\approx V_{1/2}$) will decrease when the total mobile-phase concentration increases even at constant feed composition. As shown by Table 2, the half breakthrough volume $V_{1/2}$ and the breakthrough volume V_{BK} substantially decrease with increasing total mobile-phase concentration.

In addition to flow rate and feed metal concentration, feed pH plays an important role in column dynamics [35,36]. The feed metal equivalence fraction varies with the feed pH at a constant total mobile-phase concentration:

$$x_{MF} = \frac{C_{MF}}{C} = \frac{C - C_H}{C} = \frac{C - 10^{-pH}}{C} \quad (19)$$

According to Eq. (19), the feed metal equivalence fraction increases with increasing feed pH at a constant total mobile-phase concentration. As shown by Fig. 6, the larger feed metal equivalence fraction has a lower $\Delta y_{MF}/\Delta x_{MF}$ and therefore results in a smaller breakthrough volume according to Eq. (4). Fig. 7 shows the experimental and predicted breakthrough curves of the Cu^{2+}/H^+, Zn^{2+}/H^+, and Cd^{2+}/H^+ ion-exchange systems with different feed pHs and metal concentrations. As is shown by Fig. 7b and c, the effect of feed pH can be predicted by the constant-pattern wave model successfully.

5. Conclusions

The constant-pattern wave model previously developed to predict the breakthrough curves of activated carbon adsorption systems with Langmuir or Freundlich isotherm has been modified to predict the heavy metal ion-exchange breakthrough curves. Several column experiments of copper, zinc, and cadmium with different feed metal concentrations, pHs, and flow velocities were performed and the breakthrough curves were measured. The self-sharpening wave model along with the equilibrium constant model for ion-exchange equilibrium was used to estimate the breakthrough volumes and thus to predict the breakthrough curves of the column experiments satisfactorily. However, the constant-pattern wave model considering finite mass-transfer rate provided more precise prediction of the breakthrough curves. The experimental results show that a higher total mobile-phase concentration or a higher feed pH can lead to an earlier column breakthrough. Using the correlation for the overall mass-transfer coefficient developed in this study, the ion-exchange column breakthrough curves under varying operating conditions can be successfully predicted by the constant-pattern wave model. Therefore, the constant-pattern wave model along with the equilibrium constant model can facilitate ion-exchange column design and operation.

Acknowledgement

The financial support from National Science Council of Taiwan under grant NSC93-2214-E-036-002 is highly appreciated.

References

[1] R.M. Rosain, Reusing water in CPI plant, Chem. Eng. Progr. 89 (1993) 28.
[2] J.H. Suh, D.S. Kim, Comparison of different sorbents (inorganic and biological) for the removal of Pb^{2+} from aqueous solutions, J. Chem. Technol. Biotechnol. 75 (2000) 279–284.
[3] M. Ajmal, R.A.K. Rao, R. Ahmad, J. Ahmad, L.A.K. Rao, Removal and recovery of heavy metals from electroplating wastewater by using Kyanite as an adsorbent, J. Hazard. Mater. B87 (2001) 127–137.
[4] V. Boonamnuayvitaya, C. Chaiya, W. Tanthapanichakoon, S. Jarudilokkul, Removal of heavy metals by adsorbent prepared from pyrolyzed coffee residues and clay, Sep. Purif. Technol. 35 (2004) 11–22.
[5] E. Erdem, N. Karapinar, R. Donat, The removal of heavy metal cations by natural zeolites, J. Colloid Interface Sci. 280 (2004) 309–314.
[6] J. Hanzlík, J. Jehlička, O. Šebek, Z. Weishauptová, V. Machovič, Multicomponent adsorption of Ag(I), Cd(II) and Cu(II) by natural carbonaceous materials, Water Res. 38 (2004) 2178–2184.
[7] V.J. Inglezakis, H. Grigoropoulou, Effects of operating conditions on the removal of heavy metals by zeolite in fixed bed reactors, J. Hazard. Mater. B112 (2004) 37–43.
[8] H.G. Park, M.Y. Chae, Novel type of alginate gel-based adsorbents for heavy metal removal, J. Chem. Technol. Biotechnol. 79 (2004) 1080–1083.
[9] Y. Sağ, I. Ataçoğlu, T. Kutsal, Equilibrium parameters for the single- and multicomponent biosorption of Cr(VI) and Fe(III) ions on *R. arrhizus* in a packed column, Hydrometallurgy 55 (2000) 165–179.
[10] J.P. Chen, X. Wang, Removing copper, zinc, and lead ion by granular activated carbon in pretreated fixed-bed columns, Sep. Purif. Technol. 19 (2000) 157–167.
[11] V.C. Taty-Costodes, H. Fauduet, C. Porte, Y.S. Ho, Removal of lead(II) ions from synthetic and real effluents using immobilized *Pinus sylvestris* sawdust: adsorption on a fixed-bed column, J. Hazard. Mater. B123 (2005) 135–144.
[12] J. Goel, K. Kadirvelu, C. Rajagopal, V.K. Grag, Removal of lead(II) by adsorption using treated granular activated carbon: batch and column studies, J. Hazard. Mater. B125 (2005) 211–220.
[13] N. Öztürk, D. Kavak, Adsorption of boron from aqueous solutions using fly ash: Batch and column studies, J. Hazard. Mater. B127 (2005) 81–88.
[14] K. Dorfner, Ion Exchangers, Walter de Gruvter Berlin, 1999.
[15] S.H. Lee, S. Vigneswaran, H. Moon, Adsorption of phosphorus in saturated slag media columns, Sep. Purif. Technol. 12 (1997) 109–118.
[16] A.A. Susu, Mathematical modelling of fixed bed adsorption of aromatics and sulphur compounds in kerosene deodorization, Chem. Eng. Proc. 39 (2000) 485–497.
[17] G.O. Wood, Quantification and application of skew of breakthrough curves for gases and vapors eluting from activated carbon beds, Carbon 40 (2002) 1883–1890.
[18] L.J. Bruce, H.A. Chase, The combined use of in-bed monitoring and an adsorption model to anticipate breakthrough during expanded bed adsorption, Chem. Eng. Sci. 57 (2002) 3085–3093.
[19] A. Gupta, V. Gaur, N. Verma, Breakthrough analysis for adsorption of sulfur-dioxide over zeolites, Chem. Eng. Proc. 43 (2004) 9–22.
[20] D.C.K. Ko, J.F. Porter, G. Mckay, Application of the concentration-dependent surface diffusion model on the multicomponent fixed-bed adsorption systems, Chem. Eng. Sci. 60 (2005) 5472–5479.
[21] U. Kumar, M. Bandyopadhyay, Fixed bed column study for Cd(II) removal from wastewater using treated rice husk, J. Hazard. Mater. B129 (2006) 253–259.
[22] J.M. Chern, S.N. Huang, Study of non-linear wave propagation theory. 1. Dye adsorption by activated carbon, Ind. Eng. Chem. Res. 37 (1998) 253–257.
[23] J.M. Chern, S.N. Huang, Study of non-linear wave propagation theory. 2. Interference phenomena of single-component dye adsorption waves, Sep. Sci. Technol. 34 (1999) 1993–2011.
[24] J.M. Chern, C.Y. Wu, Adsorption of binary dye solution onto activated carbon: isotherm and breakthrough curves, JCIChE 30 (1999) 507–514.
[25] J.M. Chern, Y.W. Chien, Adsorption of nitrophenol onto activated carbon: isotherms and breakthrough curves, Water Res. 36 (2002) 647–655.

[26] R.S. Juang, S.H. Lin, K.H. Tsao, Sorption of phenols from water in column systems using surfactant-modified montmorillonite, J. Colloid Interface Sci. 269 (2004) 46–52.
[27] K.R. Hall, L.C. Eagleton, A. Acrivos, T. Vermeulen, Pore- and solid-diffusion kinetics in fixed-bed adsorption under constant-pattern conditions, Ind. Eng. Chem. Fundam. 5 (2) (1966) 212–223.
[28] F. Couenne, C. Jallut, M. Tayakout-Fayolle, On minimal representation of heterogeneous mass transfer for simulation and parameter estimation: Application to breakthrough curves exploitation, Comput. Chem. Eng. 30 (2005) 42–53.
[29] B.C. Pan, F.W. Meng, X.Q. Chen, B.J. Pan, X.T. Li, W.M. Zhang, X. Zhang, J.L. Chen, Q.X. Zhang, Y. Sun, Application of an effective method in predicting breakthrough curves of fixed-bed adsorption onto resin adsorbent, J. Hazard. Mater. B124 (2005) 74–80.
[30] I.H. Lee, J.M. Chern, Ion-exchange equilibrium and column dynamics for heavy metals removal from wastewater, Asian Waterqual Bangkok Thailand, 2003, 2QHF22.
[31] F.G. Helfferich, G. Klein, Multicomponent Chromatography: Theory of Interference, Dekker, NY, New York, 1970.
[32] F.G. Helfferich, P.W. Carr, Non-linear waves in chromatography. I. Waves, shocks, and sharps, J. Chromatogr. 629 (1993) 97–122.
[33] J.M. Chern, F.C. Chang, Study of nonlinear wave propagation theory. III. Removing heavy metals from wastewater by ion-exchange process, Sep. Sci. Technol. 35 (2000) 1099–1116.
[34] T.K. Sherwood, R.L. Pigford, C.R. Wilke, Mass Transfer, McGraw-Hill, NY, New York, 1975.
[35] S. Kundu, S.S. Kavalakatt, A. Pal, S.K. Ghosh, M. Mandal, T. Pal, Removal of arsenic using hardened paste of Portland cement: batch adsorption and column study, Water Res. 38 (2004) 3780–3790.
[36] E. Malkoc, Y. Nuhoglu, Removal of Ni(II) ions aqueous solutions using waste of tea factory: adsorption on a fixed-bed column, J. Hazard. Mater. B135 (2006) 328–336.